(Received 19 March 2025, Accepted 11 May 2025, Scheduled 20 May 2025)

# Leveraging Time-Domain Signals for Multi-Tag Classification in Chipless RFID Systems Using Classifier Chains

Athul Thomas*, Midhun Muraleedharan Sylaja, and James Kurian

*Cochin University of Science and Technology, Kochi, Kerala 682022, India*

**ABSTRACT:** Chipless Radio Frequency Identification (CRFID) systems have emerged as a cost-effective and scalable solution for various identification and tracking applications. However, multi-tag classification remains a significant challenge due to overlapping signal characteristics and the absence of on-chip processing, which hinders accurate tag differentiation, increases interference, reduces classification accuracy, and necessitates advanced signal processing techniques for reliable identification. This study presents a novel machine learning-based approach utilizing a Classifier Chain-AdaBoost (CC-AdaBoost) model to improve multi-tag classification accuracy. Unlike conventional methods that rely on calibration or background subtraction, the proposed approach directly processes raw time-domain signals, enabling efficient and accurate classification of multiple tags simultaneously. The model is evaluated on simulated CRFID data, achieving an overall accuracy of 85%. Performance metrics such as accuracy, Hamming loss, Jaccard score, and F1-score are analysed to assess both overall classification performance and label-wise evaluation. Results indicate that CC-AdaBoost effectively differentiates tag classes, particularly excelling in high-confidence classifications while maintaining a balance between precision and recall. This study demonstrates the feasibility of CC-AdaBoost for real-world CRFID applications and suggests potential improvements for optimizing multi-tag recognition in complex environments.

## 1. INTRODUCTION

Chipless Radio Frequency Identification (CRFID) technology offers a cost-effective and scalable alternative to traditional barcodes and chipped RFID systems. Unlike barcodes and QR codes, which require line-of-sight scanning, or chipped RFID, which has higher manufacturing costs, CRFID operates without integrated circuits, reducing expenses while enabling real-time inventory tracking, asset monitoring, and secure access control [1, 2]. Beyond identification, CRFID supports indoor navigation in malls and airports [3] and integrates localization and sensing for environmental monitoring and condition-based tracking [4]. These capabilities position CRFID as a key enabler of next-generation identification and tracking technologies.

Recent studies have incorporated Artificial Intelligence (AI) into CRFID systems to overcome inherent disadvantages such as limited data processing capabilities, environmental susceptibility, and scalability challenges [2, 5–13]. AI enhances CRFID by enabling improved signal interpretation in noisy conditions, optimizing performance in diverse environments, and reducing reliance on manual calibration [7, 8]. In addition, AI algorithms facilitate real-time analytics and predictive insights, transforming CRFID data into actionable information [12, 13]. This integration mitigates traditional limitations while unlocking new opportunities for CRFID in dynamic inventory management, adaptive security systems, and intelligent navigation applications.

A detailed workflow for applying machine learning (ML) classification to CRFID tag identification was introduced by Jeong et al., encompassing tag design criteria, data collection for representative measurements, dimensionality reduction techniques, classifier evaluation for accurate predictions, and a thresholding method to improve prediction confidence [9]. To address misdecoding in chipless tags, Arjomandi et al. introduced two methods: generating 2-D images from side-looking aperture radar and virtual 2-D images from 1-D backscattering signals, followed by the proposal of a convolutional neural network-based decoding algorithm, which achieved high accuracy and eliminated ambiguity and false decoding [13].

The application of AI in CRFID systems is still in its early stages, with emerging AI models offering significant potential to enhance the performance of these systems and address various existing challenges. A key area where AI can have a transformative impact is in solving the multi-tag classification problem. In dense environments, the simultaneous identification of multiple tags remains a major challenge for CRFID systems, leading to issues such as signal interference and misclassification. AI techniques, particularly those focused on advanced signal processing and machine learning algorithms, can significantly improve the ability to distinguish and correctly identify multiple tags in real time. This ability to efficiently handle multi-tag scenarios is crucial for scaling up chipless RFID applications, particularly in complex environments such as warehouses, retail settings, and logistics, where numerous tags need to be identified simultaneously without errors.

Traditional multi-tag classification methods rely on signal processing [14], database lookup comparisons [15], and space-

* Corresponding author: Athul Thomas (athulthomas@cusat.ac.in).

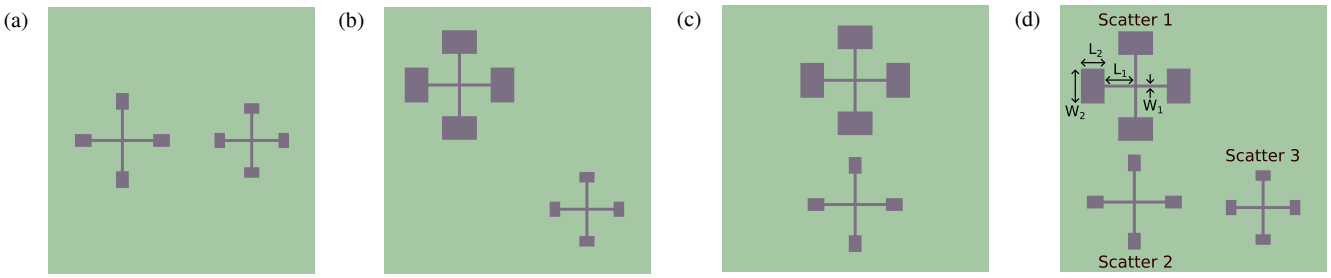


**FIGURE 1**. Chipless RFID tags used in the study, showcasing their design configurations and physical layouts. The tags include scatterers with varying resonance characteristics to enable unique identification.

division multiple access (SDMA) [16]. However, these methods face limitations such as handling widely spaced tags, restricted system capacity, and the added complexity introduced by phased array or beamforming technologies. Kheawprae et al. demonstrated the use of AI techniques for multi-tag identification in CRFID systems. This method applies a one-dimensional convolutional neural network (1D CNN) as an intelligent classifier, processing complex natural resonances (CNRs) as input data to improve detection performance and efficiency [17].

The work presented here investigates the use of multi-label classification models for precise tag classification in CRFID systems, with a particular focus on analysing the time-domain response of the tags. The research also explores the feasibility of simultaneously recognizing multiple tags, addressing a key challenge in environments where numerous tags must be identified and tracked concurrently. This study serves as a pilot investigation considering simulated responses from chipless tags, with the findings providing a foundation for future applications in practical, real-world scenarios. The insights gained can be applied to develop CRFID systems that are resilient to environmental factors such as noise and interference, paving the way for more robust and scalable real-time applications.

## 2. ANALYSIS OF BACKSCATTER SIGNAL FROM CRFID TAGS

Analysing backscatter signals from CRFID tags is crucial for accurate identification and classification. This study examines time-domain responses to extract unique features, enabling efficient multi-tag detection and improved system performance.

### 2.1. Tag Design

The tag used in this study is based on the design proposed by Sajitha et al. [18], utilizing a Stepped Impedance Resonator (SIR) for the development of a 3-bit CRFID tag operating in the 2 GHz–6 GHz range. The unique properties of SIRs, including independent control over resonant modes, the ability to place higher harmonics away from the fundamental frequency, and precise tuning of resonance characteristics, are effectively leveraged in the tag's design.

Seven distinct tags, labeled 001 to 111, are designed by arranging three different scatterers. A selection of these tags is shown in Fig. 1. The dimensions of the scatterers on each tag

**TABLE 1**. Dimensions of the scatterers used in the tag design.

| Scatterer | $L_1$ (mm) | $L_2$ (mm) | $W_1$ (mm) | $W_2$ (mm) |
|---|---|---|---|---|
| Scatter 1 | 5.27 | 3.99 | 0.5 | 5.89 |
| Scatter 2 | 5.20 | 2.83 | 0.5 | 2.16 |
| Scatter 3 | 4.52 | 1.78 | 0.5 | 2.56 |

are provided in Table 1, and the design is implemented using CST Microwave Studio. The simulated frequency-domain response, presented in Fig. 2, highlights the resonant behaviour of the tags within the 2 GHz–6 GHz range.

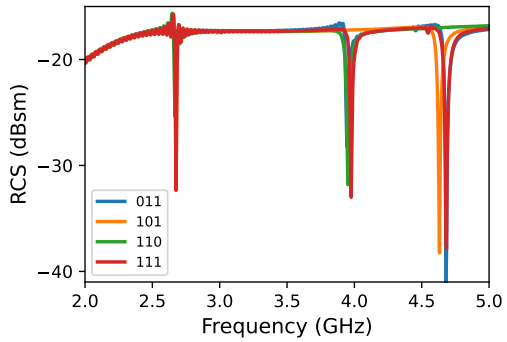


**FIGURE 2**. Frequency domain response of the tags selected for the study, highlighting the distinct resonance frequencies corresponding to the scatterers on each tag.

The configuration labeled 000 is not included, as it represents the absence of a tag rather than a distinct tag state. In a multi-tag classification scenario, the goal is to accurately identify and differentiate multiple tags based on their unique resonant characteristics.

### 2.2. Examination of Scattering Characteristics in Single-Tag Systems

A significant portion of research involving AI in CRFID systems relies on frequency-domain responses [2, 6–9, 11–13], but these systems require expensive readers with wideband Voltage Controlled Oscillators (VCO) and often require precise orientation and calibration to reduce interference from clutter and antenna coupling. To address these limitations, time-domain analysis and reading methods offer a simpler, more cost-effective

alternative that eliminates the need for complex calibration and strict alignment.

The transient analysis of the CRFID tag is performed using CST Microwave Studio simulation software. A plane wave excitation polarized along the $X$-axis is used for interrogation. The setup in CST Studio is depicted in Fig. 3. The scattered field is measured with an electric probe aligned with the polarization direction of the plane wave ($x$-axis), positioned 30 cm away from the tag to capture the response.

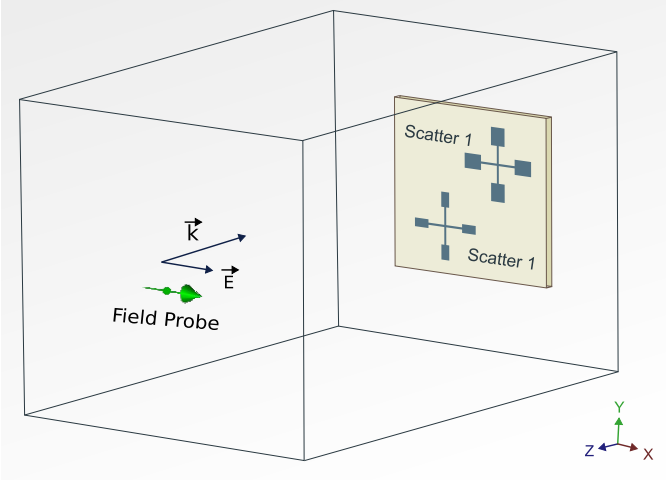


**FIGURE 3**. Simulation setup used for the transient analysis of the backscattered signal from the tag. The setup includes the interrogation signal source, the tag under test, and the receiver probe aligned along the excitation signal's polarization.

The interrogation signal used is a modulated Gaussian pulse, which can be expressed as Eq. (1):

$$X(t) = A_0 \cos(2\pi f_c t) \exp\left(-\frac{(t-\mu)^2}{2\sigma^2}\right) \tag{1}$$

where $X(t)$ is the time-domain signal, $A_0$ the amplitude, $f_c$ the carrier frequency, $\mu$ the center of the Gaussian pulse, and $\sigma$ the width of the pulse.

The reflected signal ($y_c(t)$) from the tag can be expressed as in Eq. (2) [19, 20].

$$\begin{aligned} y_c(t) = {} & A_s \cos(2\pi f_c t) \exp\left(-\frac{(t-\mu-\mu_{\text{tag}})}{2\sigma^2}\right) \\ & + \sum_{n=1}^{N} A_n \exp(a_n + j\omega_n t) + n(t) \end{aligned} \tag{2}$$

In this expression, $y_c(t)$ is the received signal at time $t$, $A_s$ the amplitude of the structural mode component, $f_c$ the carrier frequency of the excitation signal, and $\mu$ the propagation delay, while $\mu_{\text{tag}}$ accounts for the tag's position-induced delay. The Gaussian envelope, characterized by the standard deviation $\sigma$, defines the signal's temporal spread. The second term models the resonant behavior of the tag, with $A_n$ as the amplitude, $a_n$ as the damping factor, and $\omega_n$ as the resonant frequency. The imaginary unit is $j$, and $n(t)$ represents the additive noise.

Together, these components model the structural mode Radar Cross Section (SMRCS), which closely resembles the interrogation pulse, and the Tag Mode Radar Cross Section (TMRCS), which carries the unique identity of the tag.

The backscattered signal from the tag, captured by an electric field probe aligned with the polarization of the excitation signal (X direction) at a distance of 30 cm, is shown in Fig. 4. Two signals follow the shape of the transmitted signal: the first, with higher amplitude, represents the transmitted signal detected by the probe in front of the source. The SMRCS closely matches the interrogation pulse, while the TMRCS, which contains the tag ID, appears later with smaller amplitude. The duration of the TMRCS is determined by the resonators' quality factor; higher energy storage leads to a longer duration.

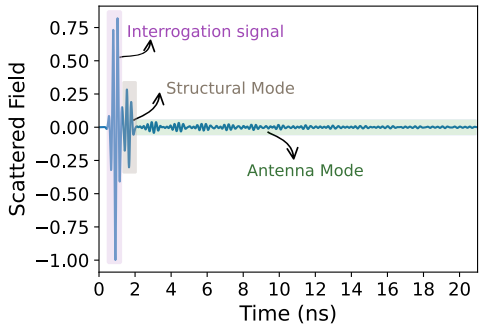


**FIGURE 4**. Signal picked up by the electric probe placed in front of the source and 30 cm away from the tag, illustrating the distinct components, including the transmitted signal, structural mode, and Tag mode responses.

To retrieve the tag ID from the time-domain data, a Fast Fourier Transform (FFT) analysis is applied. This involves windowing the transmitted signal and the structural mode component to isolate the relevant frequency components. The resulting frequency spectrum, shown in Fig. 5, highlights distinct resonances corresponding to the scatterers on the tag. These resonances are key to identifying the tag, as each scatterer produces a unique frequency signature that can be used to decode the tag's ID.

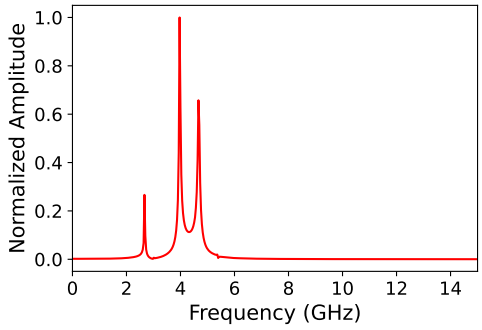


**FIGURE 5**. Normalized frequency spectrum of the Tag mode RCS filtered from the backscattered signal of a 3-scatterer tag placed 30 cm away from the source.

### 2.3. Investigation of Scattering Dynamics in Multi-Tag Systems

CRFID tag collisions can occur in two scenarios, as illustrated in Fig. 6(a) and 6(b). In the first scenario, Tag 1 and Tag 2 are

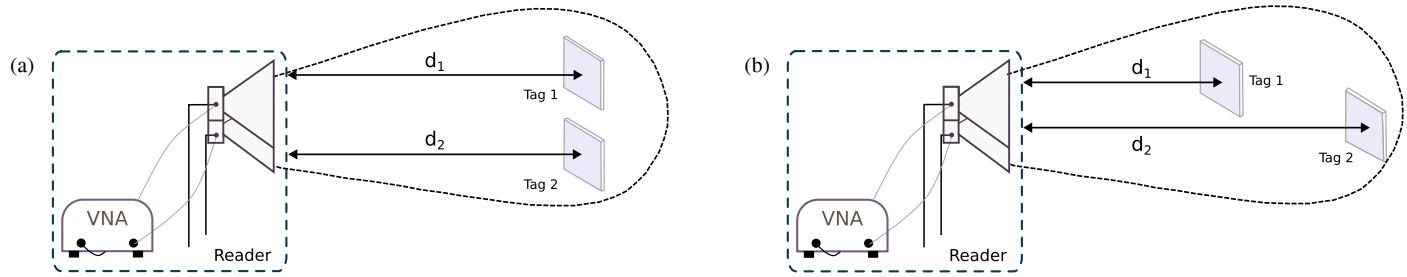


**FIGURE 6**. Scenarios illustrating chipless RFID tag collisions. (a) Tags at the same distance result in overlapping signals due to simultaneous backscatter. (b) Slight displacement introduces a time delay, reducing signal overlap and enhancing identification accuracy.

equidistant from the reader ($d_1 = d_2$), causing their responses to merge due to constructive or destructive interference, leading to classification errors or signal loss. In contrast, the second scenario introduces a slight displacement between the tags, creating a time delay that reduces signal overlap and improves separation. This study focuses on the latter, as displacement minimizes interference and enhances multi-tag detection accuracy in practical applications.

In CRFID systems, multiple tags simultaneously respond to an interrogation signal from a single reader, resulting in a superimposed received signal. The total backscattered signal, $y(t)$, from $N$ tags can be expressed as [19]:

$$y(t) = y_{\text{Tag1}}(t, \tau_{\text{Tag1}}) + y_{\text{Tag2}}(t, \tau_{\text{Tag2}}) + \cdots + y_{\text{TagN}}(t, \tau_{\text{TagN}}) + n(t) \tag{3}$$

Since each tag introduces a distinct delay $\tau_{Tagi}$, the received signal can be rewritten in a more compact summation form:

$$y(t) = \sum_{i=1}^{N} y_{Tagi}(t, \tau_{Tagi}) + n(t) \tag{4}$$

Here, $y_{Tagi}(t, \tau_{Tagi})$ represents the signal from the $i$th tag, and $n(t)$ denotes the noise introduced by environmental factors and system imperfections.

The response of each tag consists of both the structural mode radar cross section and tag mode radar cross section components. The combined signal incorporating these effects is given by [19]:

$$y(t) = \sum_{i=1}^{N} \left( A \cos(2\pi f_c t) \exp\left[ -\frac{(t - \tau_{\text{Tagi}})^2}{2\sigma^2} \right] \right) + \sum_{n=1}^{n} A_n \exp(a_n + j\omega_n t) + n(t) \tag{5}$$

In Eq. (5):

- The first summation term represents the SMRCS component, which follows a Gaussian-modulated cosine function centered at $f_c$, the carrier frequency.
- The second summation term accounts for the TMRCS contributions, incorporating complex exponential terms that capture the transient electromagnetic behavior.
- The presence of noise $n(t)$ models unwanted disturbances that may affect signal detection.

From Eq. (5), it is evident that the received signal is a mixture of multiple backscattered responses, each affected by its unique delay $\tau_{Tagi}$. If the separation between adjacent tags is greater than the system's minimum resolution, the individual tag responses can be more effectively distinguished.

Figure 7 illustrates the time-domain backscattered signals received from Tag 1 and Tag 2. The Structural Mode RCS of these tags experience delays of $\tau_{\text{Tag1}}$ and $\tau_{\text{Tag2}}$, respectively, due to differences in their spatial positions relative to the reader. These delays create temporal separation in the received signals, facilitating individual signal analysis.

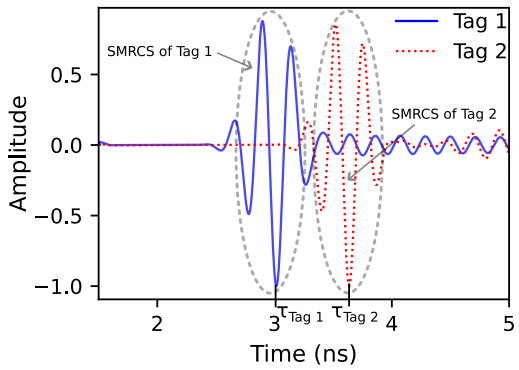


**FIGURE 7**. Time-domain backscattered signal from multiple chipless tags under interrogation, showing TMRCS and SMRCS.

This temporal distinction plays a crucial role in multi-tag classification, as it allows a machine learning model to effectively isolate and identify the response of each tag despite overlapping frequency-domain characteristics. By leveraging these time delays, the ML model can extract key transient features such as peak amplitude, decay rate, and signal envelope, enabling robust classification even in challenging scenarios where multiple tags are simultaneously interrogated.

## 3. ML METHODS

### 3.1. Data Collection

To ensure the effectiveness of AI models, a diverse and comprehensive training dataset is essential. The dataset should en-

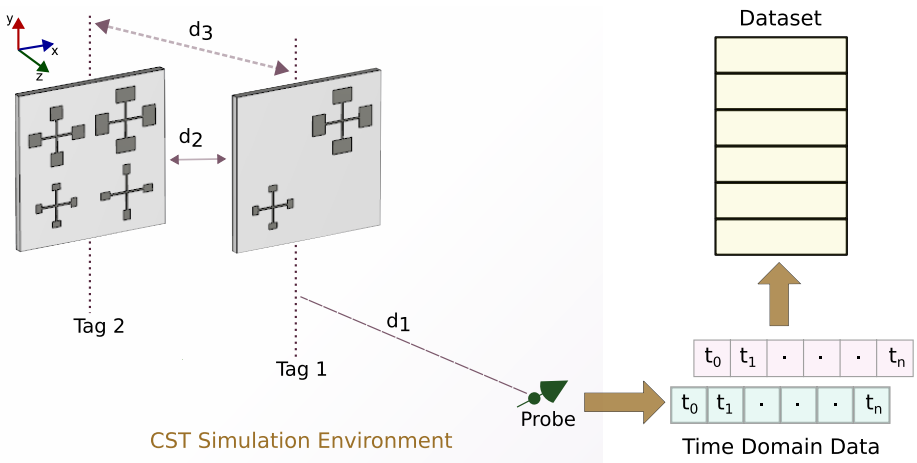


**FIGURE 8**. Block diagram of the CST simulation setup used to systematically generate datasets from various tags and their combinations.

**TABLE 2**. Number of measurements for each scenario.

| Scenario | Parameter Variation | Total Simulations |
|---|---|---|
| Scenario 1 : Individual Tag | Each of the seven unique tags (001 to 111) tested independently. $d_1$ varied from 25 cm to 60 cm in 5 cm steps. | $7 \times 8 = 56$ |
| Scenario 2: Multi-tag | Tag 1 fixed, Tag 2 ID varied across all 3-bit combinations (excluding 000). $d_1$ varied from 25 cm to60 cm in 5 cm steps, $d_3$ constant, $d_2$ fixed. | $21 \times 8 = 168$ |
| Scenario 3: Multi-tag | Tag 1 fixed, Tag 2 ID varied across all 3-bit combinations (excluding 000). $d_1$ varied from 25 cm to 60 cm in 5 cm steps, $d_3$ varied from 1 cm to 5 cm in 1 cm steps, $d_2$ fixed. | $21 \times 8 \times 5 = 840$ |

compass a broad range of time-domain responses, accounting for varying distances between tags and differing environmental conditions. This study serves as an initial exploration to assess the potential of AI models in improving CRFID systems. For the analysis, a dataset generated through simulation was employed. The data collection process is outlined in the block diagram shown in Fig. 8. Simulations were carried out using CST Microwave Studio, with an electric field probe utilized to record the backscattered signals from the tags. The interrogation signal consisted of a plane wave polarized along the $x$-axis.

Initially, the simulation was carried out considering only individual tags marked as Scenario 1 in Table 2, where each of the seven unique tags, represented by binary identifiers ranging from 001 to 111, was independently tested. The behaviour of each tag was analyzed under varying conditions by adjusting the distance $d_1$ from the interrogator as reported in Table 2. The distance $d_1$ was varied from 25 cm, positioned beyond the near-field region to ensure stable and consistent signal propagation, up to 60 cm, which was confirmed as the maximum detection range based on real-world performance measurements conducted in a controlled microwave laboratory setup.

To evaluate the performance of CRFID systems in detecting multiple tags, two primary simulation scenarios were created marked as Scenario 2 and Scenario 3 in Table 2. These scenarios involved the simultaneous detection of two tags, Tag 1 and Tag 2. Although real-world systems are typically designed to detect a larger number of tags, the practical limit is influenced by several factors. These factors include the transmitter's power, receiver sensitivity, antenna beamwidth, and the distance between the tags and interrogator, all of which influence signal strength and the potential for interference. By starting with two tags, the simulation aimed to explore the fundamental dynamics of multi-tag detection before progressing to more complex scenarios.

In Scenario 2, the experiment was designed to evaluate the performance of the system when varying the tag's identification and distance from the interrogator. Tag 1 was assigned a fixed ID, while Tag 2's ID was systematically varied across all possible 3-bit combinations, excluding "000," to simulate different tag configurations. The distance between Tag 1 and the interrogator, denoted as $d_1$, was varied within the range of 25 cm to 60 cm, allowing an assessment of how the system performs

over this distance range. Importantly, the separation between the two tags along the $z$-axis, denoted as $d_3$, was kept constant to avoid any variations in vertical positioning during the experiment. Additionally, the inter-tag distance along the $x$-axis, denoted as $d_2$, was fixed to ensure that the observed effects on performance were not influenced by horizontal tag separation. Since the identification of Tag 1 and Tag 2 is interchangeable, duplicate tag pairings (such as Tag 1 with Tag 2 or Tag 2 with Tag 1) were removed, resulting in 21 unique two-tag combinations that were analyzed in the experiment.

In Scenario 3, the primary goal was to assess the system's ability to differentiate between closely spaced tags in the presence of varying distances from the interrogator. Similar to Scenario 2, the inter-tag distance along the $x$-axis ($d_2$) was kept constant. However, in this scenario, the distance between the tags and the interrogator ($d_1$) was varied in steps from 25 cm to 60 cm, providing a more refined evaluation of how distance influences the system's ability to detect and resolve tags. Furthermore, the separation between the two tags along the $z$-axis ($d_3$) was varied from 1 cm to 5 cm. This variation was intended to evaluate the system's sensitivity to small changes in vertical positioning, which is crucial for determining whether the system can accurately detect and distinguish tags that are in close proximity to one another.

### 3.2. Data Preprocessing

The preprocessing pipeline for the CRFID tag dataset involved several key steps to ensure the model's accuracy and robustness. First, Min-Max Scaling was applied to normalize the feature values, transforming them into a uniform range between 0 and 1. This scaling process was crucial as it ensured that each feature contributed equally to the model, preventing any particular feature with a larger numerical range from dominating the learning process.

Following the scaling, the dataset was split into training and testing subsets using an 80-20 train-test split. Specifically, 80% of the data was allocated to the training set, while the remaining 20% was reserved for testing. This split ensured that the model was trained on a substantial portion of the data while also being evaluated on unseen data to assess its generalization ability.

Next, the training set ($X_{\text{train}}$) underwent data balancing using ML-SMOTE (Modified Synthetic Minority Over-sampling Technique) [21]. The training data was imbalanced, with certain label combinations appearing less frequently than others, which could negatively impact model performance. ML-SMOTE generated synthetic samples for the minority labels, ensuring that the label distribution was balanced, and the model had an equal opportunity to learn from both majority and minority labels.

### 3.3. Tag Classification Methodology

The problem of CRFID multi-tag classification involves identifying which tags are present simultaneously by analyzing their time-domain responses. This task requires a multi-label classification approach, where each instance can be associated with multiple labels. Unlike traditional single-label classification, multi-label classification must account for the relationships between labels, the high dimensionality of the output space, and potential data imbalances. These challenges necessitate specialized strategies and models to effectively capture and exploit the complex relationships within the data.

Several machine learning models can handle multi-label classification, with common problem transformation methods being Binary Relevance (BR) [22], Classifier Chains (CC) [23], and Label Powerset (LP) [24]. BR treats each label as an independent binary classification, offering simplicity but ignoring label dependencies. CC improves this by modeling interdependencies, though it is computationally expensive and sensitive to the order of classifiers. LP, which transforms the problem into multi-class classification, captures label dependencies but becomes infeasible with many labels due to exponential growth in combinations.

The Classifier Chain method was selected in this study for its ability to model inter-label dependencies. Unlike Binary Relevance, which treats each label independently, the classifier chain arranges classifiers sequentially, where each classifier predicts a label using both the original input features and the predictions of previous classifiers in the chain. This structure allows the model to exploit correlations between labels, which is particularly useful in CRFID applications, where certain tags often appear together due to shared characteristics or environmental factors.

#### 3.3.1. Training Process of the Classifier Chain

Here, the classifier chain is trained in a sequence, where each classifier predicts a specific RFID tag's presence based on time-domain features and the predictions of previous classifiers. Let's assume a dataset of $N$ samples where each sample consists of a time-domain signal as in Eq. (6) [23],

$$X^{(j)} = [x_1, x_2, \ldots, x_n] \tag{6}$$

and a multi-label vector as in Eq. (7)

$$Y^{(j)} = [y_1, y_2, \ldots, y_m], \tag{7}$$

indicating the tags detected in that particular time window. The training process works as follows: Each classifier $C_i$ is trained to predict the presence of tag $y_i$, incorporating both the time-domain features $X$ and the outputs from the previous classifiers. Specifically:

$$C_1 : X \to \hat{y}_1 \quad \text{(Tag 1 prediction)}$$

$$C_2 : (X, \hat{y}_1) \to \hat{y}_2 \quad \text{(Tag 2 prediction)}$$

$$C_3 : (X, \hat{y}_1, \hat{y}_2) \to \hat{y}_3 \quad \text{(Tag 3 prediction)}$$

$$\vdots$$

Thus, each classifier $C_i$ is trained on the feature set augmented with predictions from previous classifiers.

Classifier Chain was implemented using multiple base classifiers as shown in Fig. 9, including GradientBoostingClassifier, AdaBoostClassifier, DecisionTreeClassifier, RandomForestClassifier, and KNeighborsClassifier [25–28], to address the challenges of CRFID multi-tag classification. To optimize

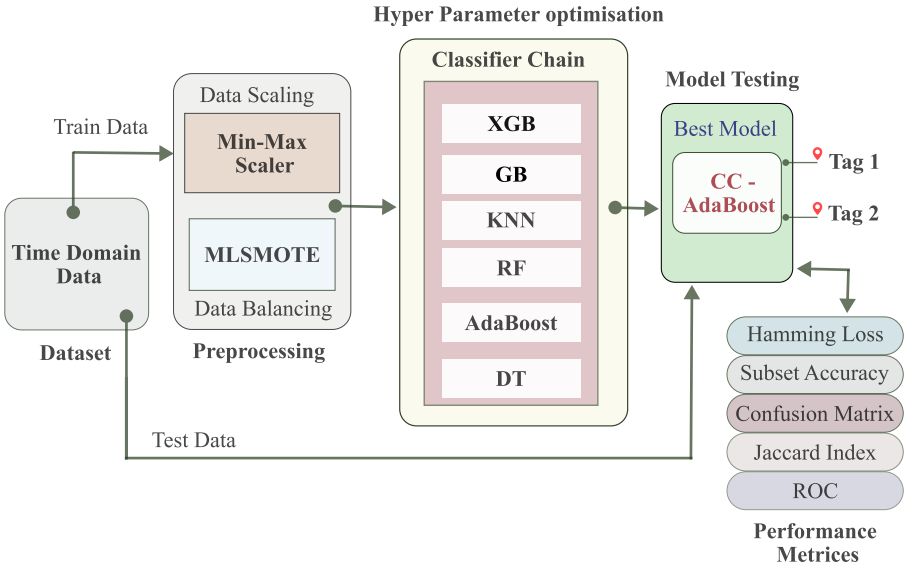


**FIGURE 9**. Block diagram illustrating the different stages of the proposed methodology, including preprocessing, parameter optimization, and model validation.

model performance, Optuna framework was utilized for systematic hyperparameter tuning. The effectiveness of different classifier combinations was evaluated using Hamming loss and F1 score as key metrics. Multiple trials with varying Classifier Chain configurations were conducted, and the results demonstrated that AdaBoostClassifier, when being combined with the Classifier Chain framework, achieved the best performance. AdaBoost's adaptive learning mechanism, which iteratively prioritizes hard-to-classify instances, contributed to a higher F1 score while effectively capturing label dependencies. Fig. 10 illustrates the parameter optimization process, showing how the number of estimators and learning rate were adjusted to enhance overall performance.

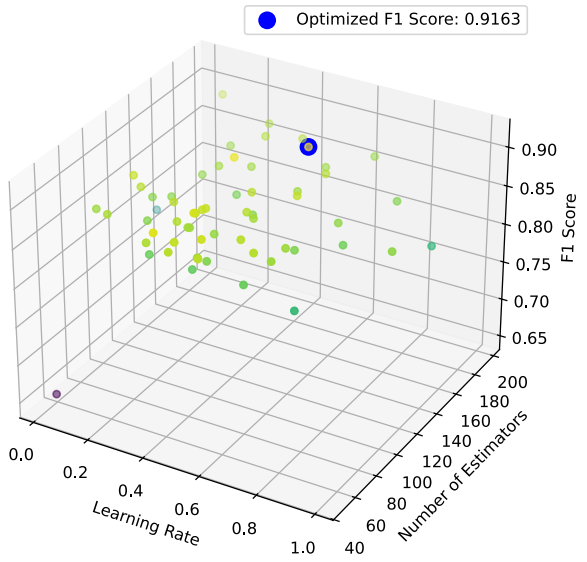


**FIGURE 10**. Parameter optimization demonstrating the impact of tuning the number of estimators and learning rate on model performance.

AdaBoost iteratively improves the accuracy of weak learners, typically decision trees (often decision stumps). It assigns weights to each training sample, where misclassified samples receive higher weights, forcing subsequent classifiers to focus more on these examples. Given a training dataset $D$ consisting of $N$ samples, where each sample is represented by a feature vector $X^{(j)}$ and its corresponding label $Y^{(j)}$, we define:

$$D = \{(X^{(j)}, Y^{(j)})\}_{j=1}^{N} \tag{8}$$

The algorithm starts with an equal weight distribution assigned to each training sample:

$$w_j^{(1)} = \frac{1}{N}, \quad j = 1, 2, \ldots, N. \tag{9}$$

At each iteration $t$, a weak classifier $h_t(X)$ is trained, and its performance is evaluated using the weighted classification error $e_t$, computed as:

$$e_t = \sum_{j=1}^{N} w_j^{(t)} I(h_t(X^{(j)}) \neq Y^{(j)}) \tag{10}$$

where $I(\cdot)$ is the indicator function, which returns 1 if the condition inside is true and 0 otherwise. The weight $\alpha_t$ assigned to classifier $h_t(X)$ is determined by:

$$\alpha_t = \frac{1}{2} \ln \left( \frac{1 - e_t}{e_t} \right) \tag{11}$$

A higher $\alpha_t$ value is assigned to classifiers with lower error rates, giving them more influence in the final decision. The weights of the training samples are then updated for the next iteration as:

$$w_j^{(t+1)} = w_j^{(t)} \exp(-\alpha_t Y^{(j)} h_t(X^{(j)})) \tag{12}$$

**TABLE 3**. Overall model performance (best values highlighted).

| Classifier | Subset Accuracy | Hamming Loss | Jaccard Score (Macro) | Precision (Macro) | Recall (Macro) | F1 Score (Macro) |
|---|---|---|---|---|---|---|
| XGBClassifier | 0.690476 | 0.07483 | 0.803571 | 0.869024 | 0.841732 | 0.850119 |
| GradientBoostingClassifier | 0.654762 | 0.078231 | 0.801587 | 0.859244 | 0.840978 | 0.847256 |
| KNeighborsClassifier | 0.428571 | 0.170068 | 0.585317 | 0.699992 | 0.635129 | 0.659251 |
| DecisionTreeClassifier | 0.440476 | 0.113946 | 0.704365 | 0.773875 | 0.802124 | 0.784779 |
| AdaBoostClassifier | **0.849135** | **0.047690** | **0.859083** | **0.912324** | **0.908154** | **0.908342** |
| RandomForestClassifier | 0.509921 | 0.091837 | 0.71131 | 0.897599 | 0.735416 | 0.796522 |

where $w_j^{(t)}$ is the weight of sample $j$ at iteration $t$, and $Y^{(j)}h_t(X^{(j)})$ determines whether the prediction is correct $(+1)$ or incorrect $(-1)$. This process is repeated until the desired number of iterations is reached. Each classifier in the classifier chain $C_i$ is an AdaBoost ensemble, enhancing robustness to variations in time-domain signals and improving generalization, particularly in the presence of noisy or incomplete RFID data.

#### 3.3.2. Prediction and Performance Considerations for RFID Multi-Label Identification

During prediction, the classifier chain generates a label set $\hat{Y} = [\hat{y}_1, \hat{y}_2, \ldots, \hat{y}_m]$ for a new RFID time-domain sample $X'$ by sequentially applying each classifier in the chain. The prediction for each tag is influenced not only by the current time-domain features $X'$, but also by the predictions of earlier classifiers in the chain. Specifically, the first classifier predicts the presence of Tag 1 ($\hat{y}_1$), and subsequent classifiers $C_2, C_3, \ldots, C_m$ incorporate these predictions as additional features.

Common metrics like accuracy and loss often fail in multi-label classification problems due to the complexities of handling multiple labels. These metrics do not account for partial correctness, as seen in CRFID systems, where a model may identify some tags but miss others. This can lead to misleading evaluations, particularly when some tags are harder to detect. To address these limitations, alternative metrics such as Hamming Loss, Jaccard Index, Subset Accuracy, and label-wise Receiver Operating Characteristic (ROC) plots are proposed.

### 3.4. Model Evaluation

In multi-label classification, model evaluation requires both overall performance and label-wise performance to ensure robust classification across all labels. Overall evaluation metrics such as accuracy, Hamming loss, and Jaccard score provide a comprehensive measure of the model's ability to predict multiple labels simultaneously. However, these metrics alone do not capture how well the model performs for each individual label. Label-wise evaluation using Confusion matrix, and ROC plots is essential to assess the model's behaviour for each tag, helping to identify any biases or inconsistencies in its predictions.

#### 3.4.1. Overall Model Performance

The comparative evaluation of models based on Subset Accuracy, Hamming Loss, Jaccard Score, Precision, Recall, and F1 Score (as detailed in Table 3) highlights significant performance differences, especially in handling multi-tag predictions.

AdaBoostClassifier demonstrated the most consistent and reliable performance across all metrics. Its high Subset Accuracy and low Hamming Loss indicate precise and complete label prediction. The strong alignment of Precision, Recall, and F1 Score further confirms its ability to maintain the balance between correctly identifying all relevant tags and minimizing false positives. This consistency makes it particularly effective in real-world multi-tag scenarios where both correctness and completeness are crucial.

XGBClassifier closely followed, showing competitive results, especially in Precision and F1 Score. While its Subset Accuracy was lower than AdaBoostClassifier, the relatively low Hamming Loss suggests that it often predicted most of the correct labels, even if not all. This implies strong performance in partially correct multi-label outputs, which is valuable in less strict applications.

GradientBoostingClassifier performed comparably to XGBClassifier, with slightly lower scores across the board. Its stable F1 Score and Jaccard Score suggest reasonable predictive accuracy, although with marginally reduced reliability in exact label combinations.

RandomForestClassifier presented mixed performance. While its Precision was high, lower Recall and F1 Score suggest a tendency toward conservative predictions—correct when being made, but often failing to capture all relevant tags. This indicates a model that may under-predict in multi-label settings, impacting overall effectiveness.

KNeighborsClassifier and DecisionTreeClassifier were the least effective. Both models had low Subset Accuracy and higher Hamming Loss, indicating frequent errors in label prediction. Their F1 Scores were also significantly lower, reflecting weaker overall classification ability. These results highlight

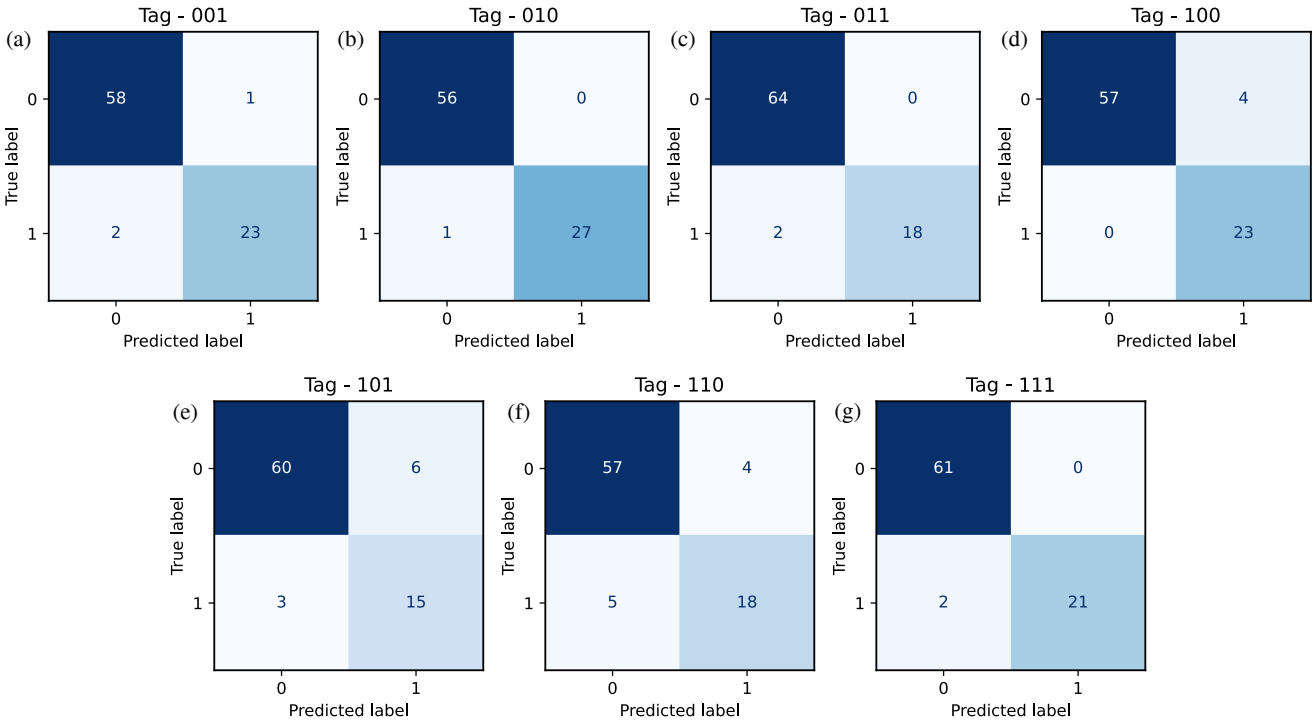


**FIGURE 11**. Confusion matrix for multi-tag classification, illustrating the prediction accuracy across seven labels (001 to 111): (a) Tag 001, (b) Tag 010, (c) Tag 011, (d) Tag 100, (e) Tag 101, (f) Tag 110, and (g) Tag 111.

their limitations in capturing complex tag relationships, especially compared to ensemble-based approaches.

In summary, AdaBoostClassifier emerged as the most suitable model, showing high and balanced scores across all evaluation metrics. Its robustness and consistency underline its strength in handling the complexity of multi-tag classification. Ensemble-based methods overall outperformed simpler classifiers, reinforcing their suitability for this task.

### *3.4.2. Label-Wise Performance Evaluation*

The evaluation of the classifier using confusion matrices demonstrates high classification accuracy across multiple tag classes in the chipless RFID system as shown in Fig. 11. The model effectively differentiates between tag signals, achieving correct classifications in the majority of cases. Notably, Class 1 (010) exhibited the most reliable performance, with minimal misclassification. Similarly, Class 2 (011) and Class 6 (111) were consistently identified with no false positives, indicating the system's strong capability to recognize these tag patterns.

However, some classes exhibited a higher tendency for misclassification. Class 4 (101) and Class 5 (110) showed more false detections, suggesting overlapping signal characteristics or feature similarities that may have led to confusion. This indicates a need for further refinement in feature extraction or classifier training to improve differentiation between these specific classes. The high number of correctly classified instances across most tag categories highlights the robustness of the approach. Addressing the misclassification patterns in certain classes could further enhance system reliability, particularly in scenarios with densely packed or closely spaced tags.

The evaluation of the classifier using receiver operating characteristic (ROC) curves and area under the curve (AUC) metrics demonstrates high classification accuracy across multiple tag classes as shown in Fig. 12. The model effectively differentiates between tag signals, achieving correct classifications in the majority of cases.

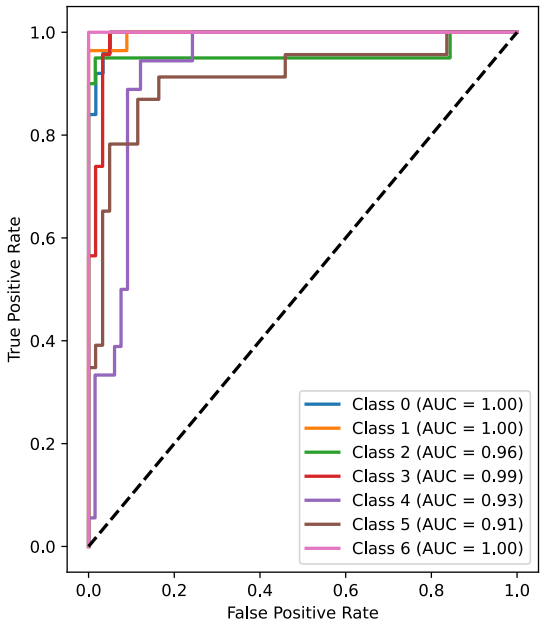


**FIGURE 12**. Receiver Operating Characteristic (ROC) curves illustrating the classifier's ability to distinguish between multiple tag classes, highlighting its predictive performance and trade-offs between sensitivity and specificity.

**TABLE 4**. Comparison of different existing techniques for CRFID tag classification.

| Ref. | Tag Size (cm) | Method | Prereq. | Bits | MT | Achievements | Limitations |
|---|---|---|---|---|---|---|---|
| [7] | 12 | LR, SVM, RF, NN, kNN | NA | 4-bit | No | Utilized raw signals for training | Small Dataset |
| [8] | 5 | SVM | NA | 5-bit | No | Used raw signal, Multiple orientations considered | Single tag detection only |
| [9] | 5 | SVM | Background subtraction | 2-bit | No | High accuracy across multiple orientations | Small dataset |
| [10] | 1.7 | LR | Background subtraction | 4-bit | No | Dimensionality reduction method, thresholding scheme | Needs background subtraction |
| [17] | 1.2 | 1-D CNN | Calibration | 3-bit | **Yes** | Multi-tag classification with good accuracy | Calibrated dataset |
| **This Study** | 4 | **CC-Adaboost** | NA | 4-bit | **Yes** | Classified multiple tags simultaneously with satisfactory accuracy | Tested only on simulation dataset |

Class 1 (010) exhibited the most reliable performance, with an AUC of 0.9968, indicating near-perfect separability. Similarly, Class 6 (111) achieved an AUC of 1.0, reflecting flawless classification with no false positives. Class 2 (011) also demonstrated strong classification performance with an AUC of 0.9570, though it exhibited some misclassification at higher thresholds.

However, some classes exhibited a higher tendency for misclassification. Class 4 (101) and Class 5 (110) had relatively lower AUC values of 0.9285 and 0.9109, respectively, suggesting a greater degree of confusion due to overlapping feature spaces. The false positive rate (FPR) for these classes increased at certain points, indicating potential misclassification with other tag categories. This suggests a need for further refinement in feature extraction or classifier training to improve differentiation between these specific classes.

Notably, Class 0 exhibited an AUC of 0.9953, with a steadily increasing true positive rate (TPR) while maintaining a low false positive rate in most cases. Similarly, Class 3 achieved an AUC of 0.9879, highlighting its strong classification capability. The trends observed across different classes indicate that the classifier effectively learns from the available training data. However, there exists a trade-off between maximizing classification confidence and minimizing misclassification, particularly for classes with similar spectral signatures.

Future optimizations may involve fine-tuning decision thresholds or employing ensemble techniques to improve classification robustness while maintaining high sensitivity and specificity. Addressing the observed misclassification trends could enhance system reliability, particularly in scenarios with densely packed or closely spaced tags.

## 4. COMPARATIVE ANALYSIS OF AI-BASED CRFID TAG CLASSIFICATION TECHNIQUES

Several studies have explored AI-based techniques for CRFID tag classification as shown in Table 4, with a primary focus on improving identification accuracy and tag recognition. Rather et al. [11] and Kheawprae et al. [17] employed 1-D convolutional neural network (CNN) models, demonstrating high accuracy but requiring calibration before each measurement, which limits real-world deployment. Similarly, Villa-Gonzalez et al. [7] and Thomas et al. [8] used traditional machine learning models such as support vector machine (SVM), Random Forest (RF), and k-Nearest Neighbor (kNN), achieving reliable classification for single-tag detection. However, these models lacked scalability for multi-tag classification. Background subtraction was another common approach, as seen in Jeong et al. [9] and Sokoudjou et al. [10], improving classification performance but adding preprocessing overhead.

In contrast, this study employs a CC-AdaBoost model, which enhances multi-tag classification without requiring calibration or background subtraction. Unlike previous works that primarily focused on single-tag identification, the proposed model effectively classifies multiple tags while maintaining high accuracy. Additionally, CC-AdaBoost leverages the sequential dependency between tags, outperforming traditional independent classifiers that ignore inter-label relationships.

## 5. CONCLUSION

This study investigates the application of Classifier Chain-AdaBoost for multi-tag classification in chipless RFID CRFID systems, addressing key challenges associated with overlapping signal characteristics and real-time recognition. The results demonstrate that CC-AdaBoost successfully classifies multiple tags with an accuracy of 85%, outperforming traditional independent classifiers by leveraging label dependencies. While certain tag classes, such as Class 1 (010) and Class 2 (011), achieved near-perfect classification, others exhibited misclassification due to feature overlap, particularly Class 4 (101) and Class 5 (110).

In terms of practical deployment, the tags were successfully identified at distances of up to 60 cm from the interrogator. The

maximum recognition distance was influenced by several factors, including transmitted power, antenna gain, receiver sensitivity, and operating frequency, which together define the effective range of the system.

Future work should explore hybrid AI models that combine multiple learning paradigms to further enhance classification performance. Additionally, real-world deployment and optimization of these techniques in practical CRFID systems will be essential to validate their effectiveness in diverse applications, such as inventory tracking, structural health monitoring, and smart environments. By advancing AI-based classification strategies, the reliability and scalability of CRFID systems can be significantly improved, paving the way for widespread adoption in next-generation internet of things (IoT) networks.

## ACKNOWLEDGEMENT

The authors would like to express their deep gratitude to the University Grants Commission, India, for providing essential funding for this research.

## REFERENCES

[1] Zhong, R. Y., C. Xu, C. Chen, and G. Q. Huang, "Big data analytics for physical internet-based intelligent manufacturing shop floors," *International Journal of Production Research*, Vol. 55, No. 9, 2610–2621, 2017.

[2] Nastasiu, D., R. Scripcaru, A. Digulescu, C. Ioana, R. De Amorim Jr., N. Barbot, R. Siragusa, E. Perret, and F. Popescu, "A new method of secure authentication based on electromagnetic signatures of chipless RFID tags and machine learning approaches," *Sensors*, Vol. 20, No. 21, 6385, 2020.

[3] Khan, S. I., B. R. Ray, and N. C. Karmakar, "RFID localization in construction with IoT and security integration," *Automation in Construction*, Vol. 159, 105249, 2024.

[4] Shen, X., G. Shi, L. Cheng, L. Gu, Y. Rao, and Y. He, "Chipless RFID-inspired sensing for smart agriculture: A review," *Sensors and Actuators A: Physical*, Vol. 363, 114725, 2023.

[5] Mulloni, V. and M. Donelli, "Chipless RFID sensors for the Internet of Things: Challenges and opportunities," *Sensors*, Vol. 20, No. 7, 2135, 2020.

[6] Rather, N., R. B. V. B. Simorangkir, J. L. Buckley, B. O'Flynn, and S. Tedesco, "Deep-learning-assisted robust detection techniques for a chipless RFID sensor tag," *IEEE Transactions on Instrumentation and Measurement*, Vol. 73, 1–10, 2023.

[7] Villa-Gonzalez, F., J. J. F. Sokoudjou, O. Pedrosa, D. Valderas, and I. Ochoa, "Analysis of machine learning algorithms for USRP-based smart chipless RFID readers," in *2023 17th European Conference on Antennas and Propagation (EuCAP)*, 1–5, Florence, Italy, Mar. 2023.

[8] Thomas, A., M. M. Sylaja, and J. Kurian, "Refinement of chipless RFID tags across multiple positions for improved recognition reliability through machine learning techniques," *Progress In Electromagnetics Research C*, Vol. 150, 57–68, 2024.

[9] Jeong, S., J. Hester, R. Bahr, and M. M. Tentzeris, "A machine learning approach-based chipless RFID system for robust detection in real-world implementations," in *2021 IEEE MTT-S International Microwave Symposium (IMS)*, 661–664, Atlanta, GA, USA, Jun. 2021.

[10] Sokoudjou, J. J. F., F. Villa-González, P. García-Cardarelli, J. Díaz, D. Valderas, and I. Ochoa, "Chipless RFID tag implementation and machine-learning workflow for robust identification," *IEEE Transactions on Microwave Theory and Techniques*, Vol. 71, No. 12, 5147–5159, 2023.

[11] Rather, N., R. B. V. B. Simorangkir, J. L. Buckley, B. O'Flynn, and S. Tedesco, "Machine learning approaches for EM signature analysis in chipless RFID technology," in *2024 18th European Conference on Antennas and Propagation (EuCAP)*, 1–5, Glasgow, United Kingdom, Mar. 2024.

[12] Pranto, T. H., M. N. Neloy, A. A. Noman, S. Wasif, M. A. Wahab, and R. M. Rahman, "Utilizing deep learning in chipless RFID tag detection: An investigation on high-precision mm-wave spatial tag estimation from 2D virtual imaging," *Journal of Information and Telecommunication*, Vol. 8, No. 3, 361–383, 2024.

[13] Arjomandi, L. M., G. Khadka, and N. C. Karmakar, "Mm-Wave chipless RFID decoding: Introducing image-based deep learning techniques," *IEEE Transactions on Antennas and Propagation*, Vol. 70, No. 5, 3700–3709, 2021.

[14] El-Hadidy, M., A. El-Awamry, A. Fawky, M. Khaliel, and T. Kaiser, "A novel collision avoidance MAC protocol for multi-tag UWB chipless RFID systems based on notch position modulation," in *2015 9th European Conference on Antennas and Propagation (EuCAP)*, 1–5, Lisbon, Portugal, Apr. 2015.

[15] El-Hadidy, M., A. El-Awamry, A. Fawky, M. Khaliel, and T. Kaiser, "Real-world testbed for multi-tag UWB chipless RFID system based on a novel collision avoidance MAC protocol," *Transactions on Emerging Telecommunications Technologies*, Vol. 27, No. 12, 1707–1714, 2016.

[16] Hester, J. G. D. and M. M. Tentzeris, "Inkjet-printed flexible mm-wave van-atta reflectarrays: A solution for ultralong-range dense multitag and multisensing chipless RFID implementations for IoT smart skins," *IEEE Transactions on Microwave Theory and Techniques*, Vol. 64, No. 12, 4763–4773, 2016.

[17] Kheawprae, F., A. Boonpoonga, and D. Torrungrueng, "Complex natural resonance-based chipless RFID multi-tag detection using one-dimensional convolutional neural networks," *IEEE Access*, Vol. 11, 138 078–138 094, 2023.

[18] Sajitha, V. R., C. M. Nijas, T. K. Roshna, R. Vivek, K. Vasudevan, and P. Mohanan, "Polarization independent chipless RFID tag," *Microwave and Optical Technology Letters*, Vol. 57, No. 8, 1889–1894, 2015.

[19] Rubayet-E-Azim, "Collision, data recovery and localisation in chipless RFID," [Online]. Available: https://bridges.monash.edu/articles/thesis/Collision_Data_Recovery_and_Localisation_in_Chipless_RFID/4669612, 2017.

[20] Nijas, C. M., "Design and development of compact chipless RFID tags with high data encoding capacity," [Online]. Available: https://d-yuthi.cusat.ac.in/xmlui/bitstream/handle/purl/5225/Dyuthi

[21] Alsabry, A., M. Algabri, A. M. Ahsan, M. A. A. Mosleh, A. A. Ahmed, and H. A. Qasem, "Enhancing prediction models' performance for breast cancer using SMOTE technique," in *2023 3rd International Conference on Emerging Smart Technologies and Applications (eSmarTA)*, 1–8, Taiz, Yemen, Oct. 2023.

[22] Das, P., Y. Thakran, S. R. N. Anal, V. Pal, and A. Yadav, "BRMCF: Binary relevance and MLSMOTE based computational framework to predict drug functions from chemical and biological properties of drugs," *IEEE/ACM Transactions on Computational Biology and Bioinformatics*, Vol. 20, No. 3, 1761–1773, 2022.

[23] Read, J., B. Pfahringer, G. Holmes, and E. Frank, "Classifier chains for multi-label classification," *Machine Learning*, Vol. 85, 333–359, 2011.

[24] Munisamy, S. D., M. Sumithra, S. Vivekanandan, and P. N. Kumar, "WITHDRAWN: Equivalence classifier chain Label power set tokenization of toxic comment multi label classification using machine learning," in *Materials Today: Proceedings*, 2021.

[25] Tsai, J.-K. and C.-H. Hung, "Improving adaboost classifier to predict enterprise performance after covid-19," *Mathematics*, Vol. 9, No. 18, 2215, 2021.

[26] Khandokar, I. A., A. K. M. M. Islam, S. Islam, S. Shatabda, *et al.*, "A gradient boosting classifier for purchase intention prediction of online shoppers," *Heliyon*, Vol. 9, No. 4, e15163, 2023.

[27] Tariq, A., J. Yan, A. S. Gagnon, M. R. Khan, and F. Mumtaz, "Mapping of cropland, cropping patterns and crop types by combining optical remote sensing images with decision tree classifier and random forest," *Geo-Spatial Information Science*, Vol. 26, No. 3, 302–320, 2023.

[28] Kumari, V. S., E. Reddy, and S. Ramesh, "Comparing the performance of support vector machine and K neighbors classifier in predicting airline passenger satisfaction with high accuracy," in *AIP Conference Proceedings*, Vol. 3168, 020013, 2024.

[29] Read, J., B. Pfahringer, G. Holmes, and E. Frank, "Classifier chains: A review and perspectives," *Journal of Artificial Intelligence Research*, Vol. 70, 683–718, 2021.